RSC Advances

PAPER

View Article Online
View Journal | View Issue

Cite this: *RSC Adv.*, 2022, **12**, 27933

Highly sensitive benzothiazole-based chemosensors for detection and bioimaging of peroxynitrite in living cells†

Yaqiong Kong, [a] Rong Wu,[a] Xiaodong Wang,[a] Guoxu Qin,[a] Fengyi Wu, [a] Chunyu Wang, [ac] Minmin Chen,[a] Nannan Wang,*[a] Qian Wang*[b] and Duojun Cao*[a]

Received 22nd July 2022
Accepted 19th September 2022

DOI: 10.1039/d2ra04549d

rsc.li/rsc-advances

It is well accepted that peroxynitrite ($ONOO^-$) plays a crucial role in various physiological and pathological processes. Thus, the detection and imaging of $ONOO^-$ *in vitro* and *in vivo* with high selectivity and sensitivity is of great significance. Here we report two simple benzothiazole-based fluorescent chemosensors, **BS1** and **BS2**. Under physiological pH, both probes could quickly sense $ONOO^-$ with a remarkable "turn-on" fluorescence signal at 430 nm. The limit of detection (LOD) of **BS1** and **BS2** toward $ONOO^-$ was 12.8 nM and 25.2 nM, respectively, much lower than the reported values. Experimental results indicated that **BS1** with a diphenyl phosphonate unit presented higher selectivity for $ONOO^-$ than **BS2**. Furthermore, based on the advantages of lower cytotoxicity and pH-stabilities of **BS1**, probe **BS1** was successfully employed to detect and image $ONOO^-$ in HepG2 cells. More importantly, we used **BS1** to successfully showcase drug-induced hepatotoxicity *via* imaging $ONOO^-$ upregulated by acetaminophen (APAP), and also evaluated the remediation effect of GSH. All the results illustrated that the fluorescent probe **BS1** has great potential for the detection of $ONOO^-$ and to further uncover the roles of $ONOO^-$ during the drug-induced liver injury (DILI) process.

1. Introduction

The liver is a very important organ in the human body, which has the function of regulating metabolism and drug detoxification.[1] Drug-induced liver injury (DILI) has always been common in clinical patients and could cause acute liver failure, which generally endangers human health and even life.[2] According to statistics, the annual incidence of DILI is approximately one in 10 000 people.[3,4] Consequently, the development of an accurate and reliable method for early diagnosis of drug-induced hepatotoxicity is necessary and beneficial. However, due to the complexity of the pathophysiological mechanisms, the early diagnosis of DILI by the Roussel Uclaf causality assessment method (RUCAM) involved some drawbacks, such as relatively cumbersome operations and delayed diagnosis, and has rarely obtained satisfactory predicted results.[5] Generally, some reports revealed that drug metabolism could cause liver injury with the generation of reactive species including reactive oxygen species (ROS) and reactive nitrogen species (RNS).[6,7] Therefore, ROS and RNS could be used as biomarkers for the early diagnosis of drug-related hepatotoxicity.[8,9]

Peroxynitrite ($ONOO^-$), a highly reactive oxygen and nitrogen species (RONS), originates from the chemical transformation between nitric oxide ($^{\bullet}NO$) and superoxide anions ($O_2^{\bullet-}$).[10–14] It has been universally known that $ONOO^-$ is not only a kind of biological endogenous oxidant but an efficient nitration agent, which could easily nitrify or oxidize amino acids like tyrosine and consume biothiols, and consequently do irreversible damage to proteins, nucleic acid and lipids.[15–19] Therefore, the level change of $ONOO^-$ in the organism could been considered as an important pathogenic indicator for early diagnosis of DILI.[17,20–24] Despite of the general recognition in the formation of $ONOO^-$ and its importance in physiological and pathological processes, it has still many difficulties in tracking and monitoring directly *in situ*. The reasons lie in dynamic changes of $ONOO^-$ concentration and short half-life time (~10 ms) in *vivo* and *in vitro* as well as mutual competition and inter-conversion among endogenous biomolecules, which make selective detection of $ONOO^-$ in intricate physiological environment more challenging.[11,25–27] Thus, given the significant role and specialty of $ONOO^-$, it is in urgent need of a reliable and effective analytical method in detecting and visualizing $ONOO^-$ in practical biological systems.

[a]*Engineering Technology Center of Department of Education of Anhui Province, Institute of Novel Functional Materials and Fine Chemicals, College of Chemistry and Materials Engineering, Chaohu University, Chaohu 238024, PR China. E-mail: 053076@chu.edu.cn; nnw1990@126.com*

[b]*Department of Radiation Oncology, China-Japan Union Hospital of Jilin University, Changchun 130000, PR China. E-mail: wangqian1991@jlu.edu.cn*

[c]*School of Information Science and Technology, University of Science and Technology of China, Hefei, Anhui 230026, China*

† Electronic supplementary information (ESI) available. See https://doi.org/10.1039/d2ra04549d

Fortunately, owing to the real-time visualization, instantaneous response, convenience and noninvasive nature, fluorescence-based techniques makes accurate and efficient determination and imaging of $ONOO^-$ possible.[28–32] Recently, much efforts have been devoted to exploiting and designing novel fluorescent $ONOO^-$ probes with excellent selectivity and sensitivity. From the recent reviews of fluorescent chemosensors for $ONOO^-$ detection, it could be concluded that these fluorescent $ONOO^-$ probes were developed based on the strong oxidation, nitration, and nucleophilicity of $ONOO^-$, which usually incorporate some particular reactive moieties into different chromophores, such as alkene,[33,34] *N*-aminophenol,[35,36] active ketone,[37–39] arylboronic esters,[40–43] organoselenium/organotellurium[44,45] and diphenyl phosphonate unit.[46,47] Taking advantage of these reactive sites, the probes would release their masked fluorescence upon attacked by $ONOO^-$, which makes them promising biosensors for $ONOO^-$ detection and imaging. However, there are also many disadvantages of sensors reported already, like poor biocompatibility, photobleaching, low sensitivity, obvious interference from other RONS, making them unsuitable for the determination of $ONOO^-$ in real bio-samples. Herein, in face of the arduous problems, it is still of great significance to exploit exquisite fluorescent $ONOO^-$ probes and uncover the biofunctions of $ONOO^-$ in living systems.

Inspired by the previous works, two simple benzothiazole-based fluorescent probes, **BS1** and **BS2**, for the detection and imaging of $ONOO^-$ in *vitro and vivo* were designed for that benzothiazole probes share the merits of high quantum yield and large Stokes shift.[48] And the two probes were easily obtained based on the condensation reaction of 2-aminothiophenol and aromatic aldehydes in the presence of catalytic amount of lanthanum(III) nitrate hexahydrate in a considerable yield under mild conditions.[49] The difference of the probes in structure is that **BS1** possesses a reactive electron withdrawing diphenyl phosphonate unit while **BS2** bears a pinacol boronic ester group for monitoring $ONOO^-$. Both probes showed excellent sensitivity and rapid response toward $ONOO^-$ in comparison with the previously reported $ONOO^-$ probes (Table S1†). However, it's worth noting that the probe **BS1** with diphenyl phosphonate unit showed better selectivity than **BS2** bearing a pinacol boronic ester group. Thus, **BS1** was then employed to monitor the fluctuation of $ONOO^-$ level regulated by antipyretic acetaminophen (APAP) drug *via* fluorescence imaging. Encouragingly, with the help of probe **BS1**, the experiments demonstrated that APAP-induced hepatotoxicity was accompanied with the up-regulation of $ONOO^-$. Moreover, the use of GSH ($ONOO^-$ scavenger) could alleviate drug-induced damage, which might open the door for the nontoxic metabolism of APAP. This study would provide a potential approach for the early diagnosis and therapy of DILI.

2. Experimental

Materials and instruments, synthesis and characterization of **BS1** and **BS2**, general procedure for spectroscopic studies, cell culture and fluorescent imaging studies were listed in the ESI.†

3. Results and discussions

3.1 Synthesis of probes BS1 and BS2

The reasonable route for preparing sensors **BS1** and **BS2** were presented in Scheme 1. Structurally, the two simple probes **BS1** and **BS2** share same benzothiazole moiety and were prepared in a similar approach where $La(NO_3)_3 \cdot 6H_2O$ served as an efficient catalyst. The concrete synthesis information was outlined in ESI.† The structures of probes **BS1**, **BS2** and intermediates involved were exactly characterized through NMR and HR-MS spectroscopy (Fig. S1–S7†).

3.2 The optical response of BS1 and BS2 toward $ONOO^-$

The response of **BS1** and **BS2** toward $ONOO^-$ were evaluated in the DMSO/PBS solution (10 μM, 25% DMSO in PBS, pH = 7.4).

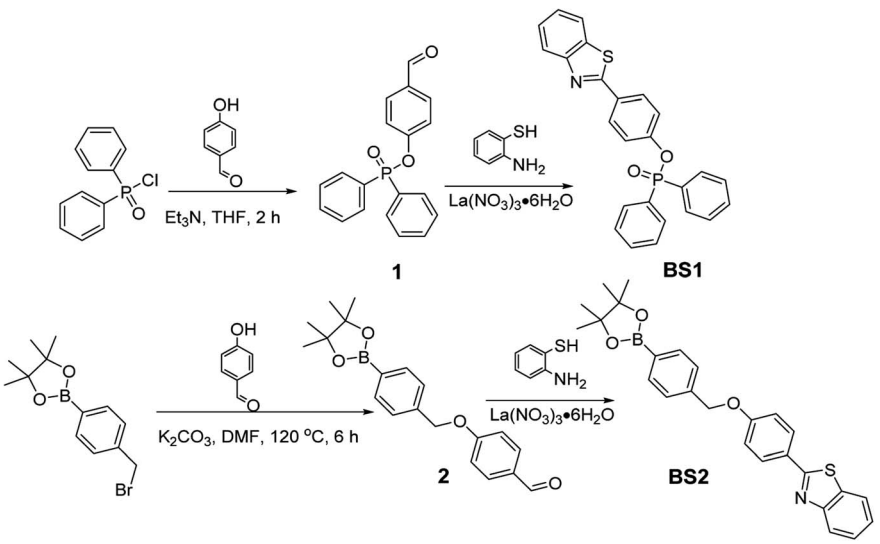

Scheme 1 Synthetic route of benzothiazole-based probe BS1 and BS2.

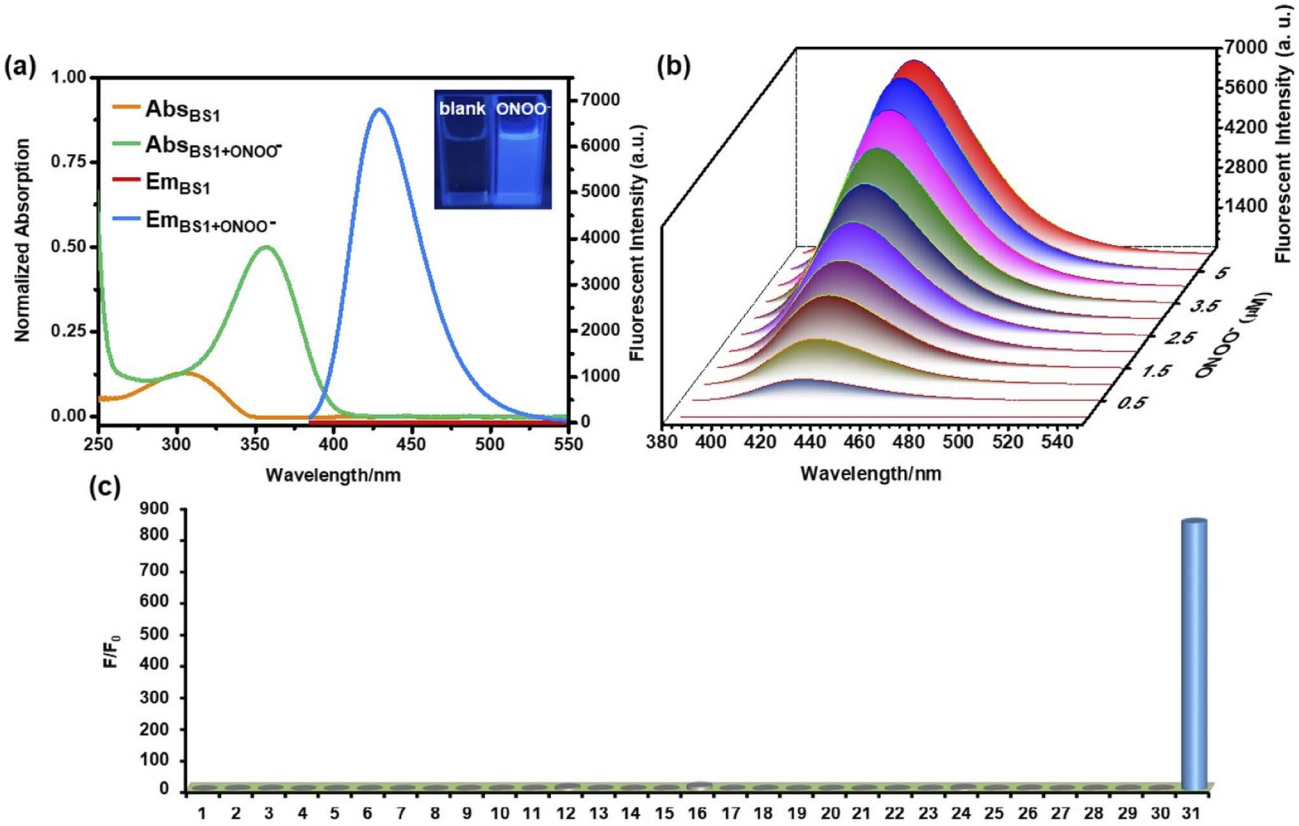

Fig. 1 (a) Absorption and fluorescence spectra of **BS1** before and after reacting with $ONOO^-$. Inset: photographs of reaction mixture in the absence (left) and presence (right) of $ONOO^-$ under 365 nm lamp. (b) Changes in fluorescence intensity of **BS1** (10 μM) upon addition of different amounts of $ONOO^-$ (0–10 μM). (c) Fluorescence response of **BS1** (10 μM) at 430 nm with various bioanalytes: (1) blank; (2) Na^+ (1.0 mM); (3) K^+ (1.0 mM); (4) Fe^{3+} (1.0 mM); (5) Zn^{2+} (1.0 mM); (6) Cu^{2+} (1.0 mM); (7) Ca^{2+} (1.0 mM); (8) Al^{3+} (1.0 mM); (9) Mg^{2+} (1.0 mM); (10) SO_3^{2-} (1.0 mM); (11) SO_4^{2-} (1.0 mM); (12) CO_3^{2-} (1.0 mM); (13) HCO_3^- (1.0 mM); (14) NO_2^- (1.0 mM); (15) NO_3^- (1.0 mM); (16) PO_4^{3-} (1.0 mM); (17) Cl^- (1.0 mM); (18) H_2S (1.0 mM); (19) GSH (1.0 mM); (20) Cys (1.0 mM); (21) Vitamin C (1.0 mM); (22) AcOK (1.0 mM); (23) $^{\bullet}OH$ (1.0 mM); (24) H_2O_2 (1.0 mM); (25) $^1O_2$ (1.0 mM); (26) NaClO (1.0 mM); (27) NO (1.0 mM); (28) TBHP (1.0 mM); (29) HNO (1.0 mM); (30) $O_2^{\bullet-}$ (1.0 mM); (31) $ONOO^-$ (0.01 mM). All data were recorded in 10 mM PBS buffer (pH = 7.4) containing with 25% DMSO. λ_{ex}: 365 nm.

As shown in Fig. 1a and S14a,† the free **BS1** and **BS2** solutions showed their maximum absorption peaks centered approximately at 305 nm and 300 nm, respectively, which could be assigned to the characteristic absorption of benzothiazole unit.[50] However, the absorption spectra exhibited apparent bathochromic shift (356 nm) when the above solutions were treated with $ONOO^-$. Furthermore, in the absence of $ONOO^-$, both of the solutions almost had no emission at 430 nm while significant fluorescence enhancement with remarkable color changing from colorless to bright blue were observed after the addition of $ONOO^-$ (insets of Fig. 1a and S14a†), which were due to the $ONOO^-$-promoted deprotection of diphenyl phosphonate group and hydrolysis of benzeneboronic ester.[43,47] Meanwhile, relative fluorescent quantum yield(Φ_F) of **BS1** and **BS2** varied from 0.05% to 48.9% and from 0.03% to 42.7%, respectively, where the ethanolic solution of anthracene (Φ_F = 27%) was used as a ref. 51. The detailed photophysical properties of **BS1** and **BS2** were listed in the Table S2.†

The concentration-dependent fluorescence titrations of **BS1** and **BS2** toward $ONOO^-$ were also investigated in the DMSO/PBS solution at ambient temperature. As seen from Fig. 1b and S14b,† upon the excitation at 365 nm, both of emission intensities gradually rose with the increasing concentration of $ONOO^-$. After addition of 6 μM $ONOO^-$ into the solution of **BS1**, the emission signaling achieved a plateau with a nearly 850-fold fluorescent enhancement (Fig. S13a†). The similar enhancement was observed for **BS2** when the concentration of $ONOO^-$ reached 10 μM (Fig. S15a†). What is noteworthy is that there were excellent linear relationships (R^2_{BS1} = 0.9989, R^2_{BS2} = 0.9980) between $ONOO^-$ concentration and emission intensities of probes (Fig. S13b and S15b†). And the limit of detection (LOD) were calculated to be 12.8 nM and 25.2 nM, respectively. Additionally, time-dependent fluorescence changes of **BS1** and **BS2** were carried out as well. The probes had a rapid response toward $ONOO^-$ and reached their equilibrium states within 300 s (Fig. S18†). And according to the formula $Ln[(F_{max} - F_t)/F_{max}] = -k't$,[52,53] their pseudo-first-order rate constants were determined as 1.49×10^{-2} s^{-1} (Fig. S19a†) and 1.23×10^{-2} s^{-1} (Fig. S19b†), respectively. Altogether, the above performances illustrated that the probes presented highly sensitive and rapid response to $ONOO^-$.

With regard to practical applications of a good chemosensor, its characteristic pH-dependent feature must be taken carefully account. The fluorescence response of **BS1** and **BS2** with and

without $ONOO^-$ under different pH conditions were investigated and the results were presented in Fig. S21.† Both solutions of free **BS1** and **BS2** kept stable and displayed nearly no emission signaling at a wide pH values varying from 2–10. However, under the same conditions, the fluorescence intensities of the solutions enhanced immediately and remarkably upon addition of $ONOO^-$, illustrating the two probes were sufficiently feasible to sense $ONOO^-$ under normal physiological environment.

3.3 Specificity of BS1 and BS2 toward $ONOO^-$

As is widely acknowledged that high selectivity is of great significance for an excellent chemosensor.[32,53] Herein, the specific recognition of **BS1** and **BS2** toward $ONOO^-$ were exactly examined in the presence of various bio-species, including cations, reactive oxygen and nitrogen species (RONS) and reactive sulfur species (RSS), *etc.*, which may influence the response efficiency of the probes for $ONOO^-$. As shown in the Fig. 1c, it could be markedly observed that the probe **BS1** presented superior response for $ONOO^-$ with notable fluorescence enhancement over other representative analytes, suggesting $ONOO^-$ triggered the cleavage of diphenyl phosphonate group of **BS1**.[54,55] Moreover, **BS2** exhibited a similar pattern as **BS1** toward $ONOO^-$ (Fig. S14c†). But, it was worth noting that H_2O_2 and NaClO could also turn on the fluorescence of **BS2** to some extent owing to hydrolysis of benzeneboronic ester induced by the two species.[56,57] Thus, it could be concluded that selectivity of probe **BS1** toward $ONOO^-$ with diphenyl phosphonate unit was superior to **BS2** bearing a pinacol boronic ester group. Afterwards, to ensure that **BS1** or **BS2** is suitable to sense $ONOO^-$ without any anti-interference of other biological substrates, the competition tests were implemented. As clearly seen from the Figs. S16 and 17,† upon introduction of $ONOO^-$ into the solutions of two probes which pretreated with corresponding competing species, the fluorescence signaling rose dramatically, indicating both probes could resist the interference of other biologically relevant species.

3.4 Investigation of the sensing mechanism

As mentioned above, the mechanism of **BS1** and **BS2** sensing $ONOO^-$ were based on the cleavage of diphenyl phosphonate group and hydrolysis of benzeneboronic ester, respectively. As a result, both **BS1** and **BS2** transformed to the same phenolic hydroxyl structure **BS-OH**. Herein, to verify our proposed reaction mechanism, high resolution mass spectrometry analysis was firstly carried out. From Figs. S6 and 7,† **BS1 and BS2** exhibited obvious peaks at $m/z = 428.0898$ and 444.1824, corresponding to [**BS1** + H^+] and [**BS2** + H^+], respectively. After interacting with $ONOO^-$, a new peak of **BS1** at $m/z = 228.0486$ was found and assigned to the compound [**BS-OH** + H^+] (Fig. S8†). For **BS2**, the peak of [**BS-OH** + H^+] at $m/z = 228.0485$ was also observed (Fig. S9†). Besides, the ^1H NMR of the reaction product for **BS1** was recorded in Fig. S10.† It was obviously found that the peak at 10.24 ppm appeared after reaction which was assigned to the phenolic proton. And also, the reaction of **BS1** with $ONOO^-$ was analyzed *via* HPLC. As shown in Fig. S11,†

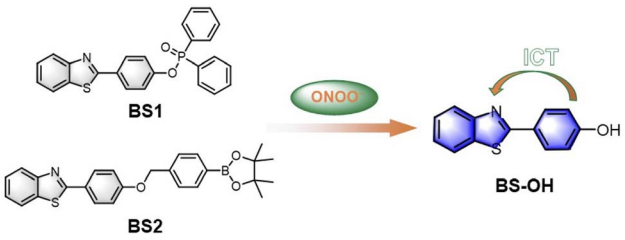

Scheme 2 Proposed recognition mechanism of **BS1** and **BS2** toward $ONOO^-$.

the probe **BS1**, **BS1** with $ONOO^-$ and **BS-OH** displayed a single peak with the retention time at 2.50 min, 1.09 min and 1.06 min, respectively. The peak of the reaction of **BS1** with $ONOO^-$ at 1.09 min in Fig. S11(b)† was in accordance with the peak of **BS-OH** at 1.06 min. For **BS2**, the FTIR analysis of **BS2** with $ONOO^-$ was collected in Fig. S12.† The FTIR spectrum of the product was identical to the spectrum based on the previous works[58,59] All the results of spectral analysis were consistent with the proposed sensing mechanism showed in Scheme 2. What's more, according to the absorption spectra analysis (Fig. 1a and S14a†), the obvious redshift of maximum peaks from 305 to 356 nm and fluorescence enhancement at 430 nm of **BS1** or **BS2** demonstrated that an intramolecular charge transfer (ICT) process happened *via* intra-molecular p–π conjugation from hydroxyl to benzothiazole unit. To further elucidate the ICT process, a density functional theory (DFT) calculation was exploited based on the Gaussian 16 program with the B3LYP/6-31G(d, p) method. From Fig. S20,† the frontier molecular orbital energies of optimized structures of **BS1**, **BS2** and **BS-OH** were calculated. Taking **BS1** as an example, in comparison with the π-electrons distribution of **BS1** and **BS-OH**, it could be clearly found that the **BS-OH** was in form of phenolate, a latent donor, which activated the ICT process from hydroxyl to benzothiazole unit. Therefore, a new push–pull conjugated system formed. And the orbital energy gaps of **BS1**, **BS2** and **BS-OH** were calculated to be 4.36 eV, 4.32 eV and 4.29 eV, respectively. Thus, the above experimental and theoretical results rationalized the sensing mechanism.

3.5 Visualizing exogenous $ONOO^-$ in living cells

Encouraged by the predominant *vitro* sensing performances of the probes, we further attempted to investigated the biosensing and bioimaging of $ONOO^-$ in living cells. Considering that probe **BS1** has much better selectivity and sensitivity, **BS1** was chosen to monitor $ONOO^-$ level in biological systems. Prior to fluorescence imaging, the cytotoxicity of **BS1** was identified by the CCK-8 assay in living HepG2 cells. From Fig. S22,† it can be seen that the cell viability was as high as 90% after incubation with **BS1** at a concentration of 100 μM for 24 h. Moreover, when the cells continued to be incubated with **BS1** for 48 h, an increased cell proliferation was observed (Fig. S23†). The above results confirmed the low cytotoxicity of **BS1** to HepG2 cells.

Subsequently, the ability of **BS1** to monitor and image exogenous $ONOO^-$ was evaluated in living HepG2 cells. Herein,

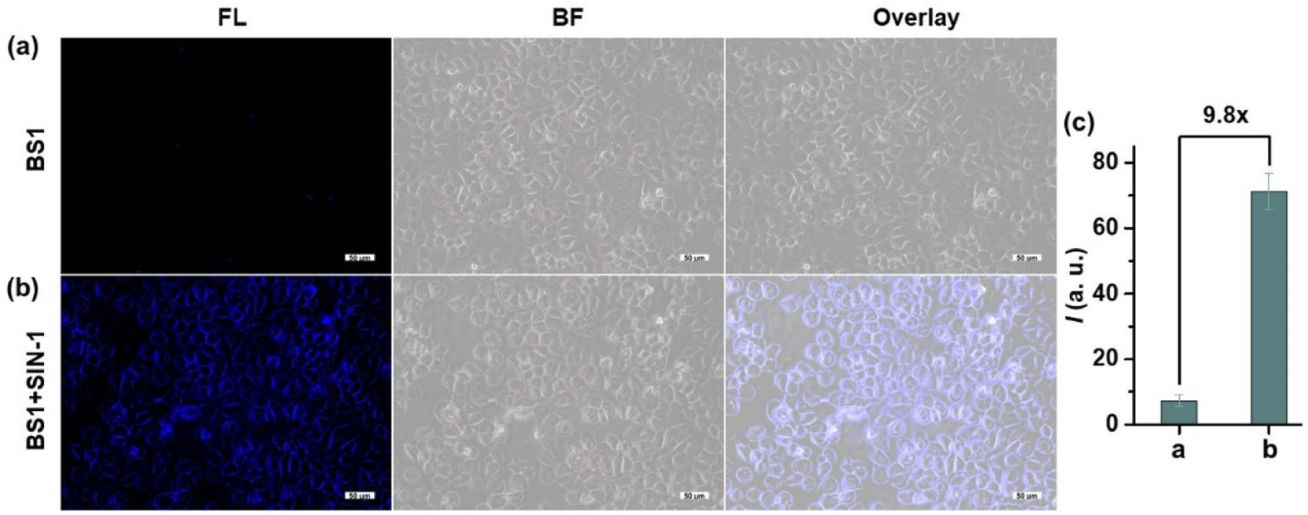

Fig. 2 Confocal fluorescence imaging of exogenous $ONOO^-$ obtained by **BS1** in HepG2 cells under different conditions. (a) Cells were incubated with **BS1** (10 μM) for 30 min at 37 °C; (b) Cells were pretreated with SIN-1 (200 μM) for 1 h, subsequently incubated with **BS1** (10 μM) for another 30 min at 37 °C. (c) Fluorescence intensity of (a) and (b). The images were obtained with 405 nm excitation and 420–490 nm collection. Scale bar: 50 μm.

3-morpholinosydnon imine hydrochloride (SIN-1) was utilized as $ONOO^-$ donor. The results were displayed in Fig. 2. In the control group, negligible fluorescence signal was detected after the HepG2 cells were incubated with **BS1**. Contrastingly, the cells which were pretreated with SIN-1 and then treated with **BS1** emitted a remarkable enhancement of intracellular fluorescence intensity in the blue channel. Furthermore, the intact cells in the bright field images implied the good viability of the HepG2 cells during the entire process of the experiment. Consequently, the data convinced that **BS1** possesses the ability of cell membrane permeability and $ONOO^-$ detection, which is promising to be a bioimaging agent for exploring $ONOO^-$ fluctuation in the physiological conditions.

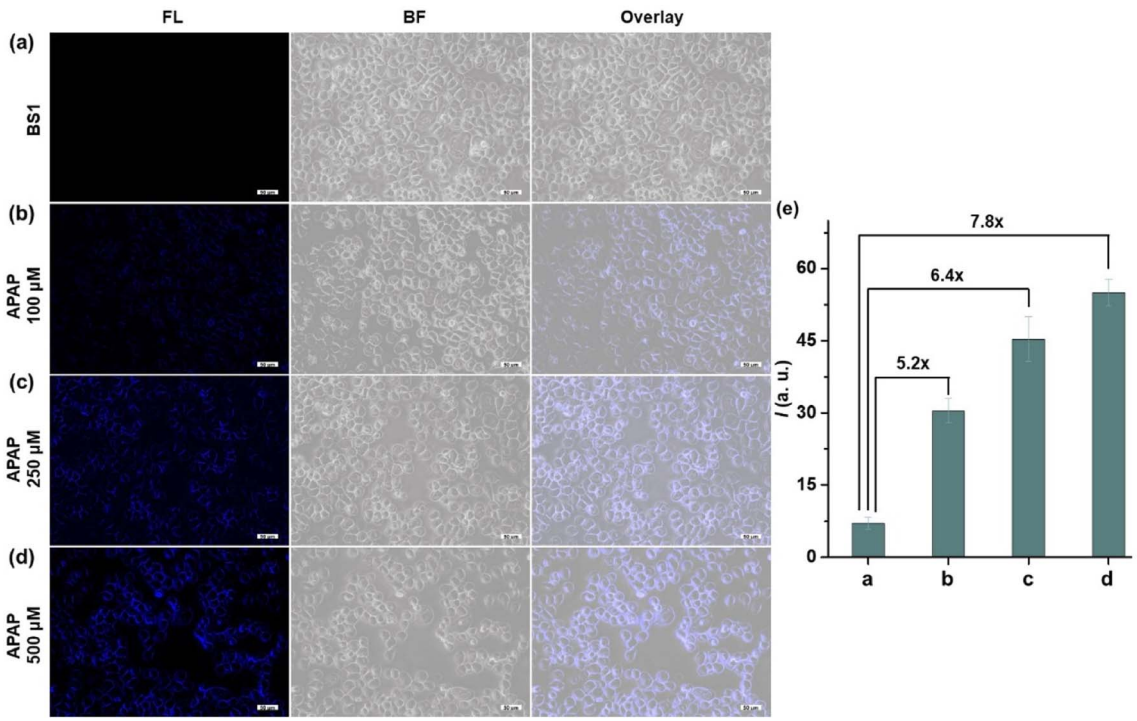

Fig. 3 Dose-dependent fluorescence imaging of APAP-induced hepatotoxicity in HepG2 cells. The cells were pretreated with (a) 0, (b) 100, (c) 250, (d) 500 μM APAP for 8 h, followed by incubated with **BS1** (10 μM) for 30 min. (e) Fluorescence intensity of (a)-(d) images. The images were obtained with 405 nm excitation and 420–490 nm collection. Scale bar: 50 μm.

3.6 APAP-induced hepatotoxicity and remediation effect of GSH

It is well-known that APAP was a common medicine to treat pain and fever. However, overdose of APAP could cause hepatotoxicity relating to excessive oxidative stress, which might be possible to induce a burst of ROS and RNS including $ONOO^-$ in the organism. Therefore, we built the dose-dependent APAP-induce injury model to confirm whether **BS1** could visualize DILI in HepG2 cells. As presented in Fig. 3, an apparent fluorescence signal in HepG2 cells was progressively enhanced by increasing the concentration of APAP (0, 100, 250, 500 μM). The obtained results not only proved that APAP-induce liver injury had a definite dose-dependent relationship, but also verified that **BS1** could be a favorable tool to reveal the upregulated $ONOO^-$ by excessive oxidative stress under APAP administration. Furthermore, as a common hepatoprotective medicine, glutathione (GSH) is an antioxidant which serves as an $ONOO^-$ scavenger in the organism. In order to validate whether GSH could alleviate the liver damage caused by APAP, the remediation experiment of GSH was performed. As shown in Fig. S24,† the group of cells treated with APAP and **BS1** exhibited an obvious blue fluorescence intensity. Meanwhile, the other group of cells were pretreated with GSH, followed by APAP, and then incubated with **BS1**. As expected, the blue fluorescence signal significantly attenuated, which could be attributed to the cell injury remediation effect *via* GSH depleting the major of endogenous $ONOO^-$. The results indicated that GSH might be an effective alternative antidote for APAP-induced liver damage. In total, **BS1** possesses the ability to be a suitable tool to visualize the diagnosis of diseases and evaluate the remediation effect of hepatoprotective drugs for DILI.

4. Conclusion

In summary, two benzothiazole-based fluorescent probes (**BS1** and **BS2**) were designed and constructed for detecting $ONOO^-$. At a physiological pH, both probes could quickly and sensitively detect $ONOO^-$ with remarkable "turn-on" fluorescence signal based on the cleavage of diphenyl phosphonate and hydrolysis of boronic pinacol ester. And nearly 850-fold signal enhancement was also found after **BS1** reacting with $ONOO^-$, and its LOD value was calculated to be as low as 12.8 nM with an excellent linear relationship. For **BS2**, the values were 695-fold and 25.2 nM, respectively. Compared with **BS2**, **BS1** bearing diphenyl phosphonate unit exhibited better selectivity and was successfully employ to detect and image $ONOO^-$ in HepG2 cells. Significantly, experiments also proved that **BS1** could monitor upregulated $ONOO^-$ levels after APAP-induced hepatotoxicity, and a remediation effect of GSH was also evaluated. These results suggested that the fluorescent probe **BS1** could be a new promising biomarker to reveal the roles of $ONOO^-$ during the DILI process.

Conflicts of interest

The authors declare no competing interests.

Acknowledgements

This work was supported by the Natural Science Foundation of Chaohu University [Grant no. XLY-202002, XLY-202212, XLY-202211], the Discipline Construction Quality Improvement Project [Grant no. kj21fdzy03]. Y. Kong would like to thank Chaohu University for the Start-Up grant [Grant no. KYQD-202006]. X. Wang would like to thank the Key Research and Development Program of Anhui Province [2022a05020019]. Q. Wang would like to thank the National Nature Science Foundation of China [Grant no. 82003208] and Science and Technology Project of Jilin Province Education Department [Grant no. JJKH20221069KJ]. M. Chen would like to thank the Natural Science Foundation of Anhui Province (Grant no. 2108085QC147). The authors thank the Shiyanjia lab (**www.shiyanjia.com**) for NMR and HRMS measurements.

References

1 A. Srivastava, J. L. Maggs, D. J. Antoine, D. P. Williams, D. A. Smith and B. K. Park, *Handb. Exp. Pharmacol.*, 2010, vol. 196, pp. 165–194.
2 L. Yuan and N. Kaplowitz, *Clin. Liver Dis.*, 2013, **17**, 507–518.
3 M. Holt and C. Ju, *Handb. Exp. Pharmacol.*, 2010, **196**, 3–27.
4 J. L. Walgren, M. D. Mitchell and D. C. Thompson, *Crit. Rev. Toxicol.*, 2002, **35**, 325–361.
5 D. J. Antoine, D. P. Williams and B. K. Park, *Expert Opin. Drug Metab. Toxicol.*, 2008, **4**, 1415–1427.
6 S. Russmann, G. A. Kullak-Ublick and I. Grattagliano, *Curr. Med. Chem.*, 2009, **16**, 3041–3053.
7 D. Pessayre, A. Mansouri, D. Haouzi and B. Fromenty, *Cell Biol. Toxicol.*, 1999, **15**, 367–373.
8 A. J. Shuhendler, K. Pu, L. Cui, J. P. Uetrecht and J. Rao, *Nat. Biotechnol.*, 2014, **32**, 373–380.
9 H. Jaeschke, G. J. Gores, A. I. Cederbaum, J. A. Hinson, D. Pessayre and J. J. Lemasters, *Toxicol. Sci.*, 2002, **65**, 166–176.
10 C. Prolo, N. Rios, L. Piacenza, M. N. Alvarez and R. Radi, *Free Radical Bio. Med.*, 2018, **128**, 59–68.
11 Z. Mao, J. Xiong, P. Wang, J. An, F. Zhang, Z. Liu and J. S. Kim, *Coordin. Chem. Rev.*, 2022, **454**, 214356.
12 L. Wang, J. Shao, B. Cheng, X. Li and J. Ma, *J. Iran. Chem. Soc.*, 2019, **16**, 437–447.
13 R. Radi, J. S. Beckman, K. M. Bush and B. A. Freeman, *J. Biol. Chem.*, 2015, **290**, 30726–30727.
14 G. Ferrer-Sueta, N. Campolo, M. Trujillo, S. Bartesaghi, S. Carballal, N. Romero, B. Alvarez and R. Radi, *Chem. Rev.*, 2018, **118**, 1338–1408.
15 P. L. Pacher, J. S. Beckman and L. Liaudet, *Physiol. Rev.*, 2007, **87**, 315–424.
16 Z. X. Chen and S. Pervaiz, *Front. Biosci.*, 2009, **14**, 4809–4814.
17 C. Szabo, H. Ischiropoulos and R. Radi, *Nat. Rev. Drug discov.*, 2007, **6**, 662–680.
18 V. Shafirovich, A. Dourandin, W. Huang and N. E. Geacintov, *J. Biol. Chem.*, 2001, **276**, 24621–24626.
19 G. Ferrer-Sueta and R. Radi, *ACS Chem. Biol.*, 2009, **4**, 161–177.

20 C. Cover, A. Mansouri, T. R. Knight, M. L. Bajt, J. J. Lemasters, D. Pessayre and H. Jaeschke, *J. Pharmacol. Exp. Ther.*, 2005, **315**, 879–887.
21 J. Li, S. Peng, Z. Li, F. Zhao, X. Han, J. Liu, W. Cao and Y. Ye, *Talanta*, 2022, **238**, 123007.
22 S. Qin, H. Lu, J. Zhang, X. Ji, N. Wang, J. Liu, W. Zhao and J. Wang, *Dyes Pigm.*, 2022, **203**, 110345.
23 S. Feng, Z. Zheng, S. Gong and G. Feng, *Sens. Actuators B Chem.*, 2022, **361**, 131751.
24 Y. Deng and G. Feng, *Anal. Chem.*, 2020, **92**, 14667–14675.
25 J. Kim, J. Park, H. Lee, Y. Choi and Y. Kim, *Chem. Commun.*, 2014, **50**, 9353–9356.
26 H. Masumoto, R. Kissner, W. H. Koppenol and H. Sies, *FEBS Lett.*, 1996, **398**, 179–182.
27 C. Ducrocq, B. Blanchard, B. Pignatelli and H. Ohshima, *Cell. Mol. Life Sci.*, 1999, **55**, 1068–1077.
28 H. Kobayashi, M. Ogawa, R. Alford, P. L. Choyke and Y. Urano, *Chem. Rev.*, 2010, **110**, 2620–2640.
29 C. Wu and D. T. Chiu, *Angew. Chem., Int. Ed.*, 2013, **52**, 3086–3109.
30 L. Wang, M. S. Frei, A. Salim and K. Johnsson, *J. Am. Chem. Soc.*, 2019, **141**, 2770–2781.
31 D. Cao, Z. Liu, P. Verwilst, S. Koo, P. Jangjili, J. S. Kim and W. Lin, *Chem. Rev.*, 2019, **119**, 10403–10519.
32 Y. Kong, X. Wan, Z. Liu, F. Chen, F. Wu, G. Qin, D. Cao and Y. Cui, *Sens. Actuators B Chem.*, 2022, **350**, 130852.
33 Z. Li, S. H. Yan, C. Chen, Z. R. Geng, J. Y. Chang, C. X. Chen, B. H. Huang and Z. L. Wang, *Biosens. Bioelectron.*, 2017, **90**, 75–82.
34 L. Wu, J. Liu, X. Tian, R. R. Groleau, S. D. Bull, P. Li, B. Tang and T. D. James, *Chem. Sci.*, 2021, **12**, 3921–3928.
35 X. Li, R. R. Tao, L. J. Hong, J. Cheng, Q. Jiang, Y. M. Lu, M. H. Liao, W. F. Ye, N. N. Lu, F. Han, Y. Z. Hu and Y. H. Liu, *J. Am. Chem. Soc.*, 2015, **137**, 12296–12303.
36 Y. Lei, W. Ren, C. K. Wang, R. R. Tao, H. J. Xiang, L. L. Feng, Y. P. Gao, Q. Jiang, X. Li, Y. Hu and F. Han, *Theranostics*, 2019, **9**, 5672–5680.
37 D. Cheng, W. Xu, L. Yuan and X. B. Zhang, *Anal. Chem.*, 2017, **89**, 7693–7700.
38 W. Wang, J. Xiong, X. Song, Z. Wang, F. Zhang and Z. Mao, *Anal. Chem.*, 2020, **92**, 13305–13312.
39 J. Zhang, X. Zhen, J. Zeng and K. Pu, *Anal. Chem.*, 2018, **90**, 9301–9307.
40 J. S. Hu, C. Shao, X. Wang, X. Di, X. Xue, Z. Su, J. Zhao, H. L. Zhu, H. K. Liu and Y. Qian, *Adv. Sci.*, 2019, **6**, 1900341.
41 D. Li, S. Wang, Z. Lei, C. Sun, A. M. El-Toni, M. S. Alhoshan, Y. Fan and F. Zhang, *Anal. Chem.*, 2019, **91**, 4771–4779.
42 H. H. Han, A. C. Sedgwick, Y. Shang, N. Li, T. Liu, B. H. Li, K. Yu, Y. Zang, J. T. Brewster, M. L. Odyniec, M. Weber, S. D. Bull, J. Li, J. L. Sessler, T. D. James, X. P. He and H. Tian, *Chem. Sci.*, 2019, **11**, 1107–1113.
43 Z. Wang, W. Wang, P. Wang, X. Song, Z. Mao and Z. Liu, *Anal. Chem.*, 2021, **93**, 3035–3041.
44 F. Yu, P. Li, G. Li, G. Zhao, T. Chu and K. Han, *J. Am. Chem. Soc.*, 2011, **133**, 11030–11033.
45 F. Yu, P. Li, B. Wang and K. Han, *J. Am. Chem. Soc.*, 2013, **135**, 7674–7680.
46 X. Luo, Z. Cheng, R. Wang and F. Yu, *Anal. Chem.*, 2021, **93**, 2490–2499.
47 R. Yuan, Y. Ma, J. Du, F. Meng, J. Guo, M. Hong, Q. Yue, X. Li and C. Li, *Anal. Methods*, 2019, **11**, 1522–1529.
48 F. Yan, J. Sun, Y. Zang, Z. Sun, H. Zhang and X. Wang, *J. Iran. Chem. Soc.*, 2020, **17**, 3179–3203.
49 K. A. Shaikh and U. N. Chaudhar, *Org. Commun.*, 2017, **10**, 288–297.
50 H. Ju, D. J. Chang, S. Kim, H. Ryu, E. Lee, I. H. Park, J. H. Jung, M. Ikeda, Y. Habata and S. S. Lee, *Inorg. Chem.*, 2016, **55**, 7448–7456.
51 W. H. Melhuish, *J. Phys. Chem. B*, 1960, **65**, 229–235.
52 L. Ji, C. Yang, H. Li, N. Yang, Y. Fu, L. Yang, Q. Wang and G. He, *Luminescence*, 2021, **36**, 4–10.
53 Y. Kong, M. Wang, W. Lu, L. Li, J. Li, M. Chen, Q. Wang, G. Qin and D. Cao, *Anal. Bioanal. Chem.*, 2022, **414**, 2009–2019.
54 Y. Wu, A. Shi, Y. Li, H. Zeng, X. Chen, J. Wu and X. Fan, *Analyst*, 2018, **143**, 5512–5519.
55 S. V. Mulay, Y. Kim, K. J. Lee, T. Yudhistira, H. S. Park and D. G. Churchill, *New J. Chem.*, 2017, **41**, 11934–11940.
56 H. Xiao, P. Li, X. Hu, X. Shi, W. Zhang and B. Tang, *Chem. Sci.*, 2016, **7**, 6153–6159.
57 E. W. Miller and C. J. Chang, *Curr. Opin. Chem. Biol.*, 2007, **11**, 620–625.
58 K. N. Patil, R. K. Bhat, C. D. Bhenki and V. B. Helavi, *Chem. Date Collect.*, 2019, **24**, 100307.
59 D. P. Araujo, V. S. S. Morais, A. Fatima and L. V. Modolo, *RSC Adv.*, 2015, **5**, 28814–28821.